



Numerical study on high-frequency effect of rail corrugation on subway-induced environmental vibrations

Sen Wang¹ · Tao Xin^{1,2} · Pengsong Wang¹ · Yi Yang¹ · Peng Chen³ · Lei Zhao⁴ · Sihe Zhao¹ · Yuming Luo¹

Received: 11 March 2022 / Accepted: 30 May 2022 / Published online: 21 June 2022
© The Author(s), under exclusive licence to Springer-Verlag GmbH Germany, part of Springer Nature 2022

Abstract

Rail corrugation is a common phenomenon in railway engineering, but its high-frequency effects on environmental vibrations are neglected in most previous research. Therefore, a hybrid numerical method was proposed in this paper to analyze subway-induced ground vibrations, especially in the high-frequency range caused by rail corrugation. The analysis model composed of a three-dimensional (3D) load generation subsystem and a two-dimensional (2D) wave propagation subsystem was established based on the vehicle-track coupling method and finite element method, and validated by the measured data. Then the high-frequency effects under different tunnel depths and rail fasteners were further studied. The results show that high-frequency vibrations propagate radially from the tunnel wall to the surrounding soil and transmit to the ground by the dominant path under different tunnel depths. The increase of tunnel depths could result in more serious high-frequency effects in the vibration amplification region. When the depth changes from 17 to 29 m, the 250 Hz ground vibration at around 30 m away from the track increases by 5.6 dB. Besides, it was found that in the commonly used range, the reduction of fastener stiffness can effectively eliminate high-frequency ground vibrations, while there is a significant nonlinear relationship between fastener damping and high-frequency vibration. The findings of this paper could provide references for parameter design in subway construction and rail corrugation remediation, and help create better living environments.

Keywords Environmental vibrations · Rail corrugation · Numerical analysis · Hybrid method · Subway · Parametric study

Introduction

Nowadays, subway-induced environmental noise and vibration are more and more prominent with the increase of operating years (Connolly et al. 2016; Sadeghi et al. 2019). As a vital factor causing this problem, the strong wheel-rail impact is closely related to track irregularities, especially the

rail corrugation which has become a common problem in railways worldwide (Oostermeijer 2008; Meehan et al. 2016).

Over the years, a great deal of research work has been made to find out how the rail corrugation formed. Wheel-rail feedback vibration (Grassie and Kalousek 1993; Grassie 2009), wheel-rail self-excited vibration (Chen et al. 2010; Kurzeck and Hecht 2010), and wheel-rail contact vibration (Jin et al. 2005; Wu and Thompson 2005) are thought to be three major generation mechanisms. Besides, through the established models and measurements (Collette et al. 2008; Eadie et al. 2008; Meehan et al. 2016; Ng et al. 2019), sleeper distance, speed distribution, and track parameters were proved to have significant influences on the rail corrugation growth. The formed rail corrugation with the dominant wavelength of 20–120 mm will cause a severe high-frequency wheel-rail impact which will lead to more annoying interior noise. Under the subway operation speed of 40–80 km/h, the significant high-frequency noise between 200 and 700 Hz in the vehicle was found to correspond to the excitation frequency caused by rail

Responsible Editor: Philippe Garrigues

✉ Tao Xin
xint@bjtu.edu.cn

- ¹ School of Civil Engineering, Beijing Jiaotong University, Beijing 100044, China
- ² Beijing Key Laboratory of Track Engineering, Beijing Jiaotong University, Beijing 100044, China
- ³ Beijing Urban Construction Design & Development Group Corporation Limited, Beijing 100037, China
- ⁴ Beijing General Municipal Engineering Design & Research Institute Corporation Limited, Beijing 100082, China

corrugation (Liu et al. 2011; Zhao et al. 2017; Feng et al. 2018).

Although high-frequency effects of rail corrugation are dominant, many field measurements (Sanayei et al. 2013; Qi et al. 2019) and simulation studies (Lopes et al. 2014, 2016; Xu et al. 2015; Kouroussis et al. 2017) proved that subway-induced environmental vibrations were mainly concentrated in the low-frequency range below 100 Hz, except that indoor vibrations may peak near 200 Hz due to structural resonance. However, it should be noted that the measured data is only responsible for the specific case and affected by many factors, including track conditions, tunnel depths, rail fasteners, and so on. It means that there may be no rail corrugation on the rail surface at all, or high-frequency vibrations caused by slight rail corrugation were attenuated greatly through tracks, tunnels, and soil layers. And for numerical simulations, it is well known that calculation results are completely determined by the model parameters. The track irregularities (Kouroussis et al. 2014; Kuo et al. 2016; Yang et al. 2017) used to calculate excitation loads were usually obtained from the track spectrum only considering medium-long wavelengths. What is more, even if the rail roughness with a wavelength less than 1.0 m measured using a CAT trolley (Jin et al. 2018) or simulated by the Sato spectrum (Xu et al. 2015) was considered, it does not mean that there must be rail corrugations. Besides, the adopted Rayleigh damping coefficients (Shih et al. 2017; Xing et al. 2019) determined by the target frequencies which were set below 100 Hz may reduce high-frequency vibration responses. The results obtained through both field measurements and numerical simulations are reasonable for certain scenes in environmental vibration assessments and predictions. But it is undeniable that chosen parameters in some simulation studies may underestimate the high-frequency environmental vibrations caused by rail corrugation.

Due to the fact that human perception of environmental changes is increasing with the people's rising living improvements, high-frequency environmental vibrations may also affect the human auditory system and nervous system (Sroczyński et al. 1978; Sutinen et al. 2007). In order to improve the living environment quality and reduce the risk of high-frequency vibration influence, the high-frequency environmental vibration should also be prevented and controlled. In this paper, a hybrid numerical model considering rail corrugations was firstly proposed to reproduce high-frequency ground vibrations presented in the authors' previous findings (Xin et al. 2020). Then more in-depth theoretical analysis was further carried out, where transmission and variation characteristics of high-frequency vibrations caused by rail corrugation under different tunnel depths and rail fasteners were analyzed. The results can

provide a theoretical reference for the remediation and prevention of high-frequency environmental vibrations caused by the subway.

Numerical analysis method

The hybrid numerical method adopted here is based on the two-step approach. For reproducing high-frequency environmental vibrations, mesh sizes of the numerical model must meet the propagation requirements of the short vibration wave, which means larger calculation time and computational resources compared with common subway-induced vibration problems. In order to balance the accuracy and efficiency, the vibration system is divided into two subsystems which are co-simulated through fastening forces in the modeling strategy, as shown in Fig. 1. The 3D load generation subsystem is coupled by the vehicle, track, and equivalent foundation, which is used to obtain the fastening forces. Then the forces are directly applied in the 2D wave propagation subsystem composed of the track, tunnels, and different soil layers to reproduce the high-frequency vibrations and study their characteristics.

Load generation subsystem

When a train runs on the track, the wheel-rail interaction forces will change randomly due to track irregularities and deformations, and further affect fastening forces in both the time domain and frequency domain. In order to consider these influencing factors, the train and the track are spatially coupled through the wheel-rail contact in the load generation subsystem, as shown in Fig. 2. What is more, the foundation including base slabs, the tunnel, and soil layers are simplified as uniformly distributed viscoelastic elements (Xing et al. 2019; Yang et al. 2019), not only exerting a supporting effect but also aiming to save the huge computation time.

The vehicle is composed of seven rigid bodies including one car body, two bogies, and four wheelsets, which are connected by the first suspension and the second suspension. All the structures except for the suspensions are represented by the lumped mass ignoring their elastic deformation, while the suspensions are simulated by the spring-damper system. In the vehicle model, 31 degree-of-freedom (DOFs) are considered. The car body and each bogie contain 5 DOFs including transverse, vertical, rolling, pitching, and yawing. And the wheel-set contains 4 DOFs except for pitching. The motion equation of the vehicle running at a constant speed is established by the Hamilton method and finally expressed as Eq. (1).

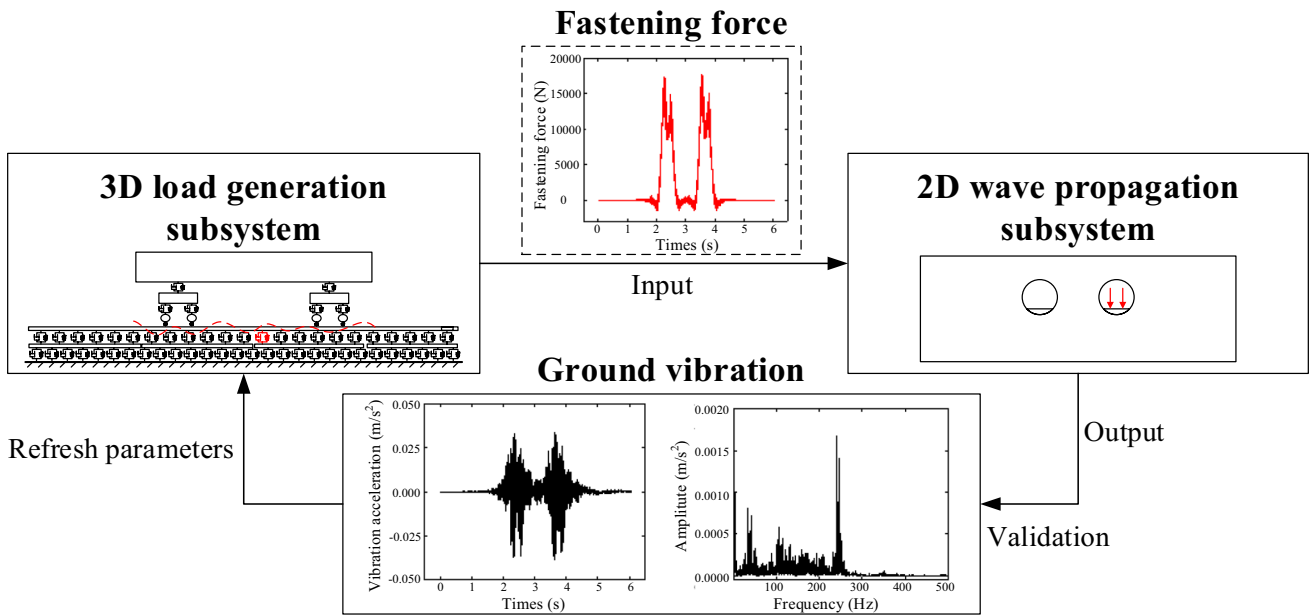


Fig. 1 Diagram of the solution of the hybrid numerical method

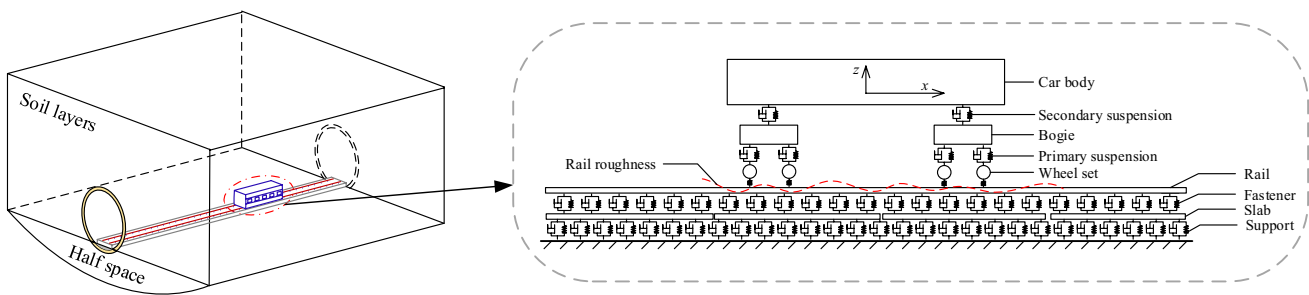


Fig. 2 Front diagram of the load generation subsystem model

$$\begin{bmatrix} M_c & 0 & 0 \\ 0 & M_b & 0 \\ 0 & 0 & M_w \end{bmatrix} \begin{Bmatrix} \ddot{\delta}_c \\ \ddot{\delta}_b \\ \ddot{\delta}_w \end{Bmatrix} + \begin{bmatrix} C_{ll} & C_{cb} & C_{cw} \\ C_{bc} & C_{bb} & C_{bw} \\ C_{wc} & C_{wb} & C_{ww} \end{bmatrix} \begin{Bmatrix} \dot{\delta}_c \\ \dot{\delta}_b \\ \dot{\delta}_w \end{Bmatrix} + \begin{bmatrix} K_{cc} & K_{cb} & K_{cw} \\ K_{bc} & K_{bb} & K_{bw} \\ K_{wc} & K_{wb} & K_{ww} \end{bmatrix} \begin{Bmatrix} \delta_c \\ \delta_b \\ \delta_w \end{Bmatrix} = \begin{Bmatrix} 0 \\ 0 \\ Q_{wr} \end{Bmatrix} \quad (1)$$

where M , C , and K refer to the matrix of mass, damping, and stiffness, respectively; subscript c , b , and m stand for the car body, the bogie, and the wheelset, respectively; δ , $\dot{\delta}$, and $\ddot{\delta}$ represent displacement, velocity, and acceleration vector, respectively; and Q_{wr} denotes the wheel-rail contact forces.

The track system is composed of rails, fasteners, track slabs, and foundations. The rails are simulated by the beam elements based on the Timoshenko beam theory, while track slabs are modeled by the solid elements with the

consideration of the actual size. The fasteners and foundations are modeled by the linear spring-damper elements, where the equivalent stiffness of foundations is determined by static calculation to obtain the same structural displacements compared with the complete system. The motion equation of the track system is expressed as Eq. (2).

$$\begin{bmatrix} M_r & 0 \\ 0 & M_s \end{bmatrix} \begin{Bmatrix} \ddot{\delta}_r \\ \ddot{\delta}_s \end{Bmatrix} + \begin{bmatrix} C_{rr} & C_{rs} \\ C_{sr} & C_{ss} \end{bmatrix} \begin{Bmatrix} \dot{\delta}_r \\ \dot{\delta}_s \end{Bmatrix} + \begin{bmatrix} K_{rr} & K_{rs} \\ K_{sr} & K_{ss} \end{bmatrix} \begin{Bmatrix} \delta_r \\ \delta_s \end{Bmatrix} = \begin{Bmatrix} Q_{rw} \\ 0 \end{Bmatrix} \quad (2)$$

where subscript r and s represent the rail and the slab, respectively.

The wheel-rail contact theory plays an important role in coupling the vehicle and track models. The wheel-rail creep force is realized by Kalker’s linear theory and nonlinearly corrected by Shen’s theory, while the wheel-rail normal force is based on the nonlinear Hertz elastic contact theory.

Most particularly, when the rail surface is affected by rail corrugation, a high level of the wheel-rail contact force can be experienced. This may lead to that the wheel losing contact with the rail, and the wheel-rail normal force is zero. Considering this possibility, the wheel-rail normal force is calculated by Eq. (3).

$$P(t) = \left\{ \frac{1}{G} [\delta_{wi}(t) - \delta_{ri}(t) - \delta_{0i}(t)] \right\}^{1.5}, \delta_{wi}(t) - \delta_{ri}(t) \geq \delta_{0i}(t) \tag{3}$$

where G represents the contact coefficient depending on the wheel-rail curvatures (Mazilu 2010); $\delta_{wi}(t)$ is the vertical displacement of the i th wheel at time t ; and $\delta_{ri}(t)$ is the vertical displacement of the rail under the i th wheel at time t . $\delta_{0i}(t)$ denotes the track irregularity on the rail surface under the i th wheel at time t , which is composed of the short-wavelength and medium-long wavelength random irregularities.

After the complete system matrices are assembled, the static analysis is first performed to obtain the initial condition for the subsequent dynamic analysis. And then the dynamic responses of tracks are calculated using Newmark- β integration method with the integration step of 5×10^{-5} s to ensure convergence of results. Further, the vertical fastening forces at any position can be obtained by Eq. 4.

$$f_i = k_0(z_{up,i} - z_{down,i}) + c_0(\dot{z}_{up,i} - \dot{z}_{down,i}) \tag{4}$$

where z and \dot{z} denote vertical displacement and acceleration; k_0 and c_0 are stiffness and damping of the i th rail fastener; and the subscript *up* and *down* represents the up node and down node of the i th rail fastener.

Wave propagation subsystem

The problem of subway-induced environmental vibrations is simplified as a 2D plane strain problem, under the condition that the soil deformation can be considered as linear elastic (Shen 2007) and satisfy the requirements of displacement coordination between different layer interfaces.

Therefore, the wave propagation subsystem is modeled by the 4-node plane strain elements, according to the typical section of track-tunnel-soil system, as shown in Fig. 3. The model size ($h \times w$) is large enough to satisfy the literature criteria that the horizontal truncation length is more than 10 times the outer diameter of tunnel on both sides (Huang et al. 2017) and the depth should be more than 6–7 times the tunnel buried depth (Zhang 2002; Shen 2007). Furthermore, the effects of model size on the target vibrations need to be investigated to determine the finally optimal size. The mesh size meets the requirement of at least 6 elements per wavelength (Shih et al. 2016), whose specific information is listed in the “Validation of established model” section. To avoid the reflection of vibration waves on the intercepted boundary surface, the artificial viscoelastic boundary is adopted and discretized by spring-damper elements with the stiffness and damping determined through the method proposed by Liu et al. (2006).

In this paper, the Caughey damping (Hall 2018; Han et al. 2021) is adopted to both cover the dominant frequency range of subway-induced vibrations below 100 Hz and high-frequency components induced by rail corrugations above 200 Hz. The damping matrix with four frequency points can be expressed as Eq. (5).

$$[C] = a_0[M] + a_1[K] + a_2[K][M]^{-1}[K] + a_3[K][M]^{-1}[K][M]^{-1}[K] \tag{5}$$

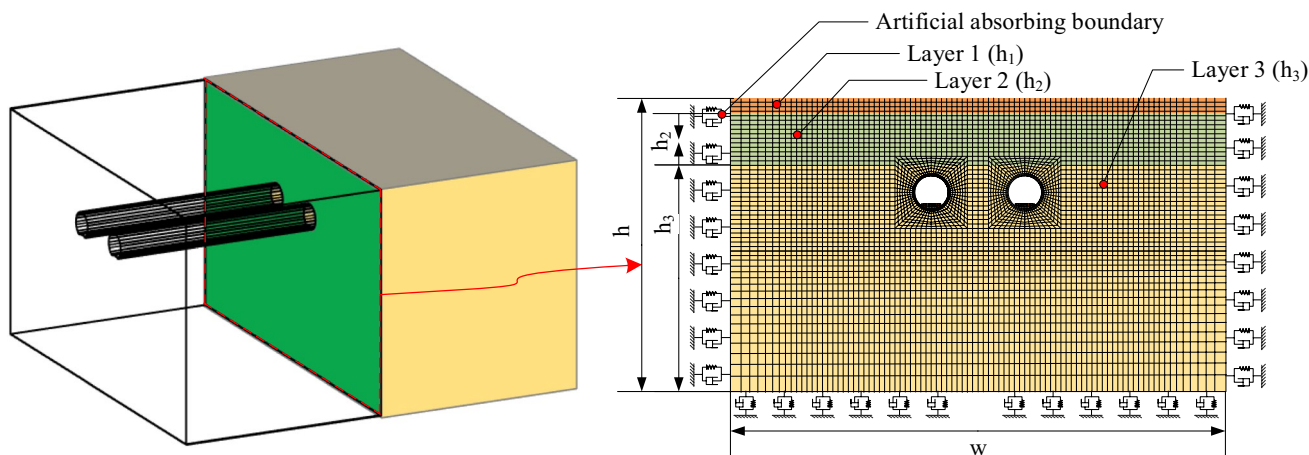


Fig. 3 Diagram of the wave propagation subsystem model

where $a_0, a_1, a_2,$ and a_3 are the coefficient related to damping ratio and characteristic frequency.

The damping ratio at n th mode can be expressed as Eq. (6), which is assumed as constant in this study. So if the damping ratio and the characteristic frequencies are obtained, the above coefficient can be calculated through simultaneous equations and the system damping is further determined.

$$\zeta_n = \frac{a_0}{2\omega_n} + \frac{1}{2}a_1\omega_n + \frac{1}{2}a_2\omega_n^3 + \frac{1}{2}a_3\omega_n^5 \tag{6}$$

where ζ_n and ω_n are the damping ratio and natural frequency at n th modal, respectively.

Besides, how to transfer the fastening forces generated by the 3D load generation subsystem into equivalent excitations used in the 2D wave propagation subsystem is a crucial concern for the reasonable simulation results. The vertical fastening forces corresponding to the typical subway section are applied in the model, and this method is proved to efficiently analyze the qualitative behavior of the vertical subway-induced environmental vibrations, as specified in the “Validation of established model” section.

Once the motion equation of the wave propagation system is established, environmental vibrations are solved by Newmark- β method with the integration step of 5×10^{-4} to cover the high-frequency vibration responses.

Validation of established model

In the case reported in China (Xin et al. 2020), serious rail corrugations with a wavelength of 40 mm were found on the right rail surface through field measurements, which far exceed the limits specified in ISO 3095 (ISO 3095–2005

2005), as shown in Fig. 4. More seriously, the high-frequency vibrations at 250 Hz caused by rail corrugation were further found in the living environments, which affected the nearby residents. On the background of this case, the hybrid numerical model of the complete environmental vibration system was established by the proposed method and verified by measured data of ground vibrations.

Model parameters

The vehicle on the operation is a B-type metro train with a running speed of about 35 km/h, with detailed parameters shown in Table.1. For the track irregularity, the short-wavelength random irregularity below 0.5 m is the measured rail corrugation shown in Fig. 4, while the medium-long wavelength irregularity is based on the fifth-grade power spectral density formula proposed by the US Federal Railroad Administration (Xing et al. 2019; Zhu et al. 2020), whose wavelength is in the range of 0.5–200 m.

The track structure is composed of 60 kg/m rail, compressed fasteners, and the common monolithic track.

Table 1 Key parameters of China’s B-type subway vehicle

Parameters	Unit	Value
Mass of car body	kg	18,250
Mass of bogie frame	kg	3393
Mass of wheel-set	kg	1527
Vertical stiffness of primary suspension	MN/m	10
Vertical stiffness of secondary suspension	MN/m	0.257
Vertical damping of primary suspension	kN-s/m	10
Vertical damping of secondary suspension	kN-s/m	30

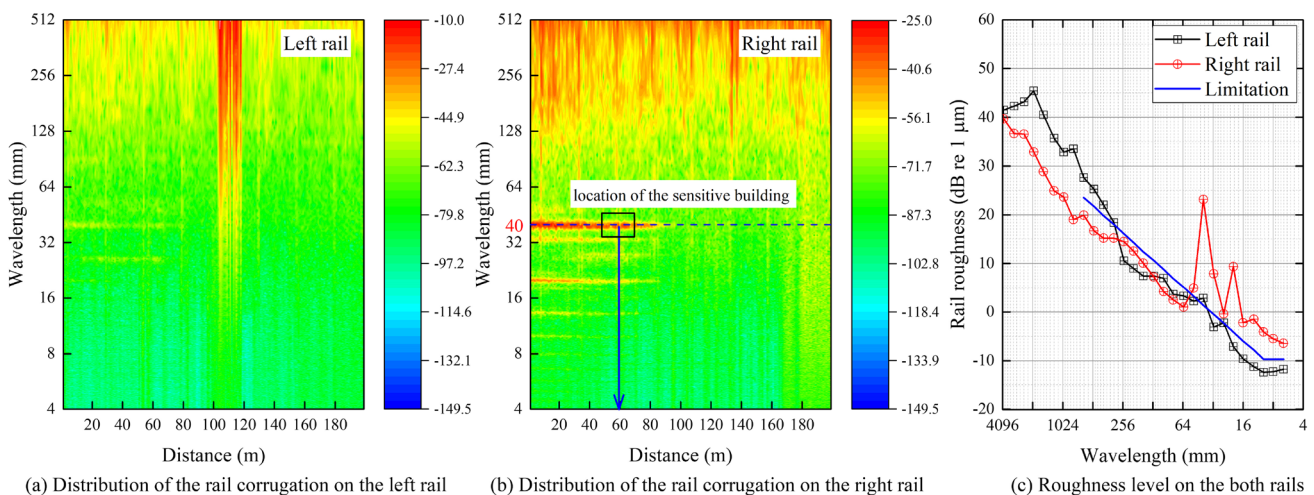


Fig. 4 Rail corrugation obtained by field measurement. (a) Distribution of the rail corrugation on the left rail. (b) Distribution of the rail corrugation on the right rail. (c) Roughness level on the both rails

The vertical stiffness of the fastener is 27 kN/mm according to test results, with the damping of 40 kN·s/m. The transverse and longitude stiffness are set to 10 kN/mm, with the damping of 2 kN·s/m. The track slabs with the width of 2400 mm and height of 300 mm adopt a continuous layout ignoring the influence of slab joint. The materials of the track slab and basement slab are C60 concrete and C40 concrete. The vertical stiffness of the structure under track slabs in load generation subsystem model is set to 80 kN/mm according to the static calculation, with the damping of 50 kN·s/m.

The tunnel whose inner and outer diameters are 5.5 m and 6.2 m adopts C50 concrete, and the buried depth is 17.5 m, as shown in Fig. 5. The soil is mainly composed of medium-soft-soil and divided into three layers. The range of 2.5 m below the surface is artificial fill, and that of 2.5–11 m is silty sand 1, while the silty sand 2 is below 11 m. The specific parameters of different soil are listed in Table 2.

The wave propagation subsystem model is in the size of 200 m × 160 m whose width is 32 times the diameter of the tunnel and height is 9 times the tunnel depth. The maximum element size of the slab, tunnel, and near-field surrounding soil is about 0.06 m which satisfies the wave propagation requirements of 250 Hz vibration under the minimum shear wave velocity of 125.1 m/s, while the mesh sizes of the far-field soil are between 0.06 and 1 m. Besides, the damping ratio of the system at different modal is set to 3% determined by the main soil type (Liu et al. 2002; Chen and Liu 2004). And ω_n is set to 1 Hz, 80 Hz, 200 Hz, and 300 Hz

considering that the ground vibration in this case is mainly in the range of 1–80 Hz and 200–300 Hz, respectively.

Comparison results

In order to have a comprehensive comparison, the simulation results and measured data (averaged by 20 groups) are compared in the one-third octave band center frequencies of 31.5 Hz, 40 Hz, 50 Hz, and 250 Hz, which can be calculated by Eq. (7).

$$VAL_i = 20 \log_{10} \left(\frac{a_i}{a_0} \right) \tag{7}$$

where a_i is the acceleration root mean square value with center frequency f_i in 1/3 octave frequency band and the reference acceleration a_0 is equal to 10^{-6} m/s^2 .

The vertical vibration levels at four positions, including 22.5 m, 30 m, 37.5 m, and 45 m, are shown and compared in Fig. 6. It can be seen that the vibration attenuation trends at different central frequencies obtained from simulation and measurement are basically consistent, showing first decreases and then increases with the increase of distance away from the track. Moreover, the simulation results are basically consistent with the measured data in the intersection of 50 Hz and 250 Hz vibration curves. However, the numerical simulation results are lower than the measured data because the load in the model is only taken from a set of fastener forces without considering the influence of other fasteners (Xu et al. 2015). The other difference may

Fig. 5 Cross-section of the tunnel structure. (a) Tunnel in the scene. (b) Tunnel in design (mm)

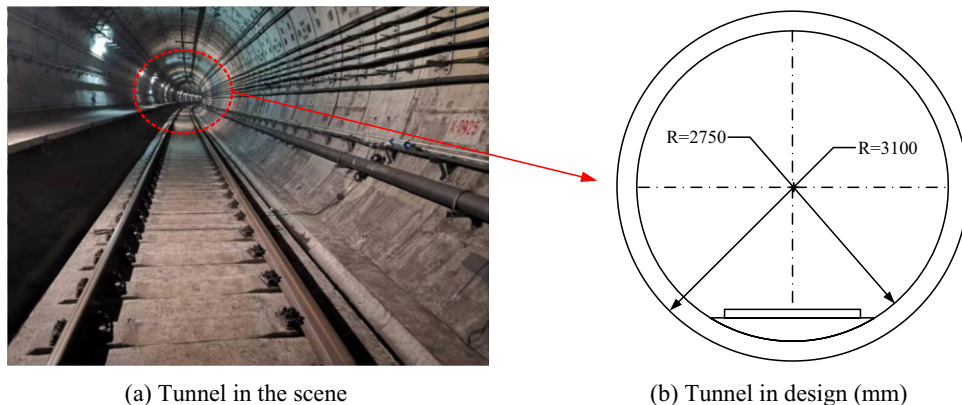
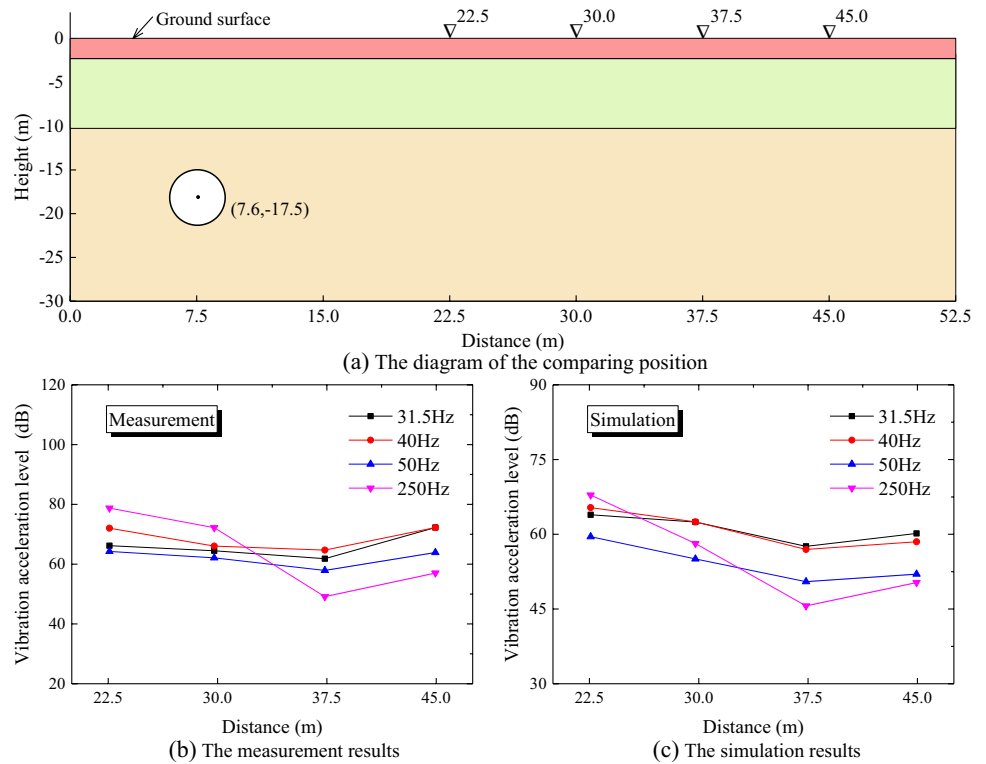


Table 2 Parameters of soil in different layers

Soil type	Elastic modulus (MPa)	Poisson ratio	Density (kg/m ³)	Shear wave velocity (m/s)	Compression wave velocity (m/s)
Artificial fill soil	86.5	0.49	1850	125.1	790.8
Silty sand 1	197.5	0.49	1900	187.7	1357.2
Silty sand 2	285.7	0.49	1910	224.6	1505.8

Fig. 6 The vibration levels at different frequency band. (a) The diagram of the comparing position. (b) The measurement results. (c) The simulation results



be due to the fact that the simulation model fails to fully consider the change of actual soil parameters. In general, it can be concluded that the model established in this paper can accurately analyze vibration propagation qualitatively, including both low frequency and high frequency.

High-frequency ground vibration

In order to have a more comprehensive understanding of high-frequency environmental vibrations caused by the presented rail corrugation, the impacts on ground vibration under different tunnel depths and rail fasteners are further analyzed through the validated numerical model. The vibration transmission and variation characteristics under different parameters are obtained, in which the rail corrugation adopts the data shown in Fig. 4. The results are helpful to determine sensitive range on the ground and select mitigation measures, so as to get a better prevention and control effect.

The effect of tunnel depth

Tunnel depth is one of the key design parameters in different subway lines. Besides, for the specific line, its buried depth changes greatly with the line direction. Therefore, it is necessary to discuss high-frequency environmental vibrations when rail corrugation occurs in different tunnel depths. Four

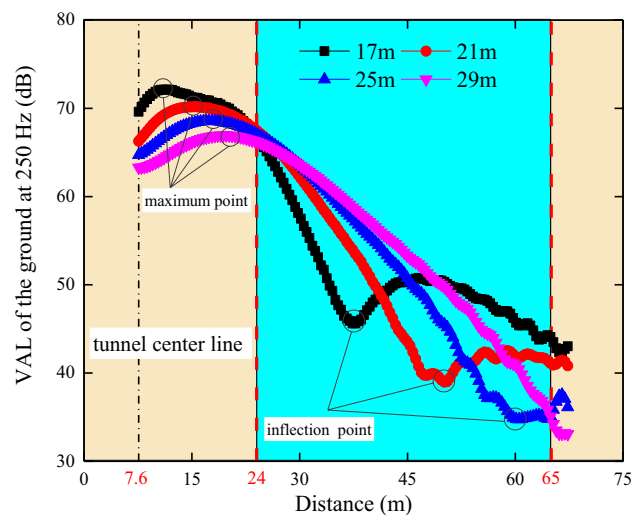


Fig. 7 Ground vibration at 250 Hz under different buried depths

tunnel depths, including 17 m, 21 m, 25 m, and 29 m, are selected for analysis in this section. The distributions of the ground vibration at 250 Hz are shown in Fig. 7.

The results show that the attenuation law of high-frequency vibration at 250 Hz is similar under different tunnel depths. Specifically, the vibration first increases, then decreases, then increases and decreases again at last along with the transverse distance. To better describe the changes, two special positions are defined. The first one is called the

maximum point, which is at the position of the peak value, while the second one is at the position of vibration mutation, called the inflection point, which is actually caused by vibration amplification (Jin et al. 2005; Ma et al. 2014). Under the buried depth of 17 m, the maximum point does not appear above the tunnel, instead, it is located near 8.5 m, and the vibration inflection point appears near 36 m. The comparisons show that with the increase of tunnel depths, the positions of the maximum point and the inflection point will shift to the right, and the vibration response at its position will also be significantly reduced. With the tunnel depth increasing from 17 to 29 m, the maximum point moves from 11.5 to 19.8 m, and the maximum value decreases from 72 to 67 dB with a reduction rate of 7.0%. With the buried depth increasing from 17 to 25 m, the inflection point moves from 37.8 to 60.5 m, and the vibration response decreases from 45.6 to 34.7 dB, which is reduced by 23.9%. The deviation may aggravate the high-frequency environmental vibration within the range from 24 to 65 m on the ground surface.

To have a more comprehensive understanding of the influence of tunnel depth on the subway-induced ground vibrations, the comparison results with consideration of the 31.5 Hz, 40 Hz, 50 Hz, and 250 Hz of the two typical positions at 22.5 m and 30.0 m are shown in Fig. 8. For the position at 22.5 m, it can be found that the ground vibrations at different frequencies decrease obviously, but high-frequency vibrations at 250 Hz are always the dominant components. Although the main component is low-frequency vibration at the position of 30 m when the tunnel depth is 17 m, the 250 Hz vibration plays a more important role with the increases of tunnel depth due to the amplification phenomenon of high-frequency vibrations presented in Fig. 7. For example, the high-frequency vibration at around 30 m away from the track increases by 5.6 dB when the depth changes from 17 to 29 m.

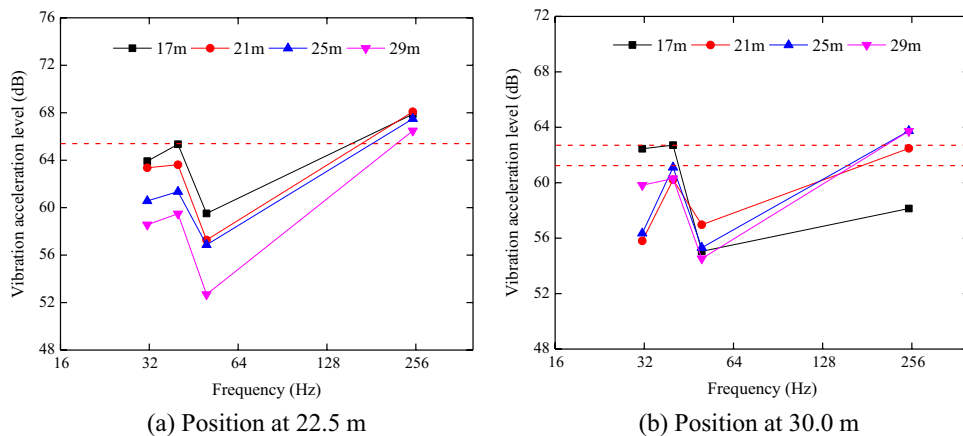
Through the above analysis, it can be concluded that the increase of tunnel depth does not mean that it can reduce the influence of high-frequency vibration at any position, on the

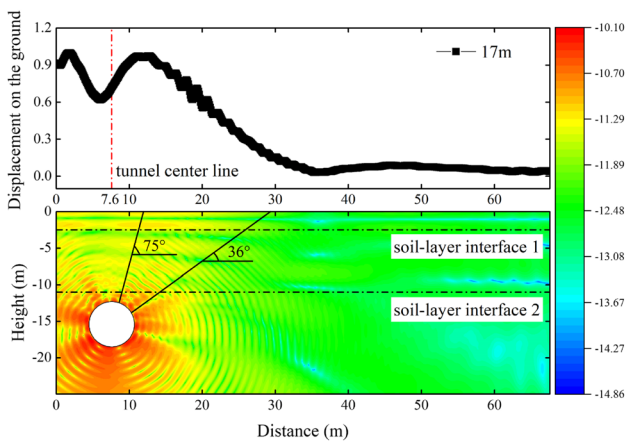
contrary, it may amplify vibrations. Therefore, for the new subway lines, the tunnel depth should be reasonably selected according to the actual placement of the environmentally vibration-sensitive buildings to prevent the possible impact of high-frequency vibration. On the other hand, the subway section with deeper tunnel depth in the operation line may also be affected by high-frequency vibration, to which attention should also be paid to.

To further explore the characteristics of high-frequency vibration propagation at different tunnel depths, the harmonic response analysis method is used for the analysis of the ground vibrations under 250 Hz excitation. As shown in Fig. 9, the up sub-graph refers to the vertical displacement of the ground, which is normalized due to the small value. The down sub-graph represents the spatial distribution of high-frequency vibration, which is processed by logarithmic due to the large difference among different regions.

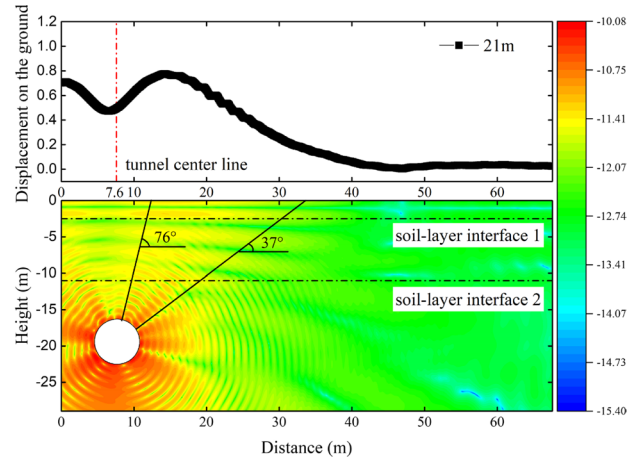
It can be seen that at different buried depths, high-frequency vibration at 250 Hz propagates radially from the tunnel wall to the surrounding soil and forms multiple vibration dominant transmission paths. The ground vibration is mainly affected by the black line path, as shown in the figure. The angle between the boundary of the transmission path and the horizontal direction basically remains unchanged at different buried depths, and the left and right are about 75° and 35°, respectively. With the increase of the tunnel depth, the position of the vibration transmitted to the ground gradually moves to the right, resulting in the deviation of the maximum point and the inflection point. Although the increase of tunnel depths can effectively reduce the maximum value of the high-frequency vibration on the ground, the main influence area of high-frequency vibration increases. In the case that the tunnel depth increases from 17 to 29 m, the main influence range increases from 17 to 30 m, resulting in the increase of vibration in this area. Therefore, the influence of tunnel depth can be attributed to the combined effect of the increase of propagation distance and the offset of propagation position.

Fig. 8 Vibration changes under different tunnel depths. (a) Position at 22.5 m. (b) Position at 30.0 m

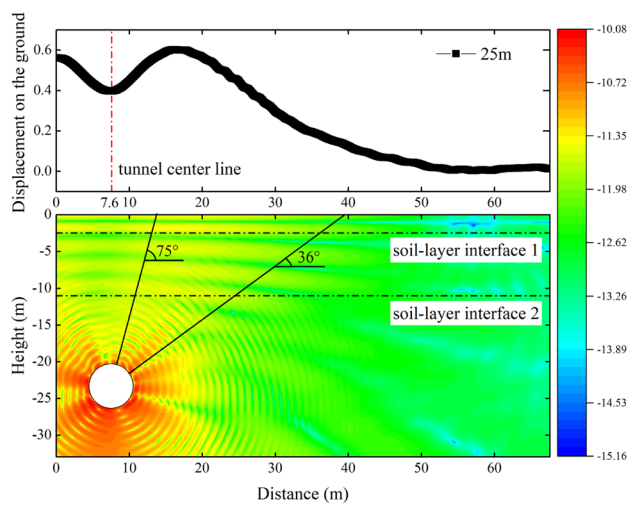




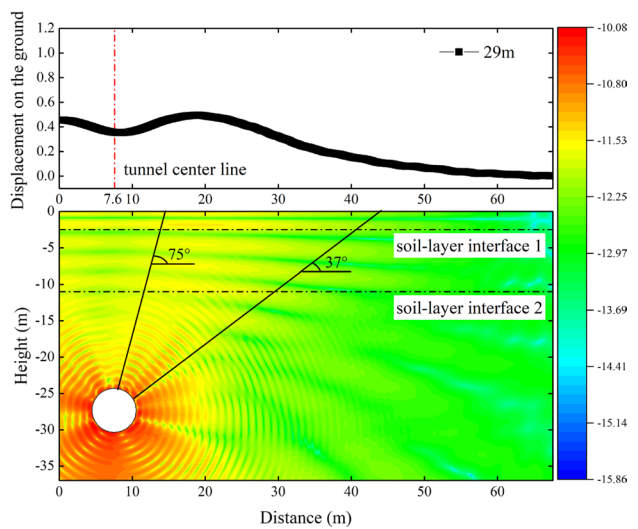
(a) Vibration distribution under 17 m



(b) Vibration distribution under 21 m



(c) Vibration distribution under 25 m



(d) Vibration distribution under 29 m

Fig. 9 Vibration distribution under different tunnel depths. (a) Vibration distribution under 17 m. (b) Vibration distribution under 21 m. (c) Vibration distribution under 25 m. (d) Vibration distribution under 29 m

Table 3 Parameters of different rail fasteners

Type	Vertical stiffness (kN/mm)	Vertical damping (kN·s/m)
DTVI2	35	10
Cologne-egg	12	1.3
Lord	25	30
Vanguard	5	10

The effect of rail fastener

With different kinds of rail fasteners, serious rail corrugation with the dominant wavelength of 30–80 mm may occur on

the rail surface. In this section, four types of fasteners widely used in subway lines are selected, including DTVI2 fastener, Cologne-egg fastener, Lord fastener, and Vanguard fastener, whose specific vertical parameters are shown in Table 3.

The distribution characteristics of high-frequency vibrations on the ground are compared and analyzed, as shown in Fig. 10. It can be seen that under the same rail corrugation, the attenuation laws of high-frequency environmental vibration with different fasteners are basically the same, but there are obvious differences in specific response values. The vibration curves of DTVI2 fasteners and Cologne-egg fasteners almost coincide. Compared with the other two fasteners, the vibration responses at any positions are the largest except for those near the inflection point, that is, up to 74.3 dB. The high-frequency vibration of the Lord

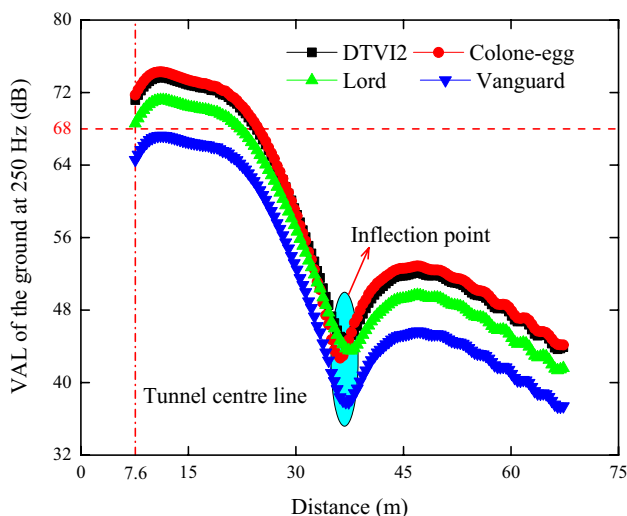


Fig. 10 Ground vibration at 250 Hz under different rail fasteners

fastener is between that of DTVI2 fasteners and Vanguard fasteners, which may exceed that of DTVI2 fasteners near the inflection point, while Vanguard fasteners show an excellent damping performance that the high-frequency vibration at different positions is at the lowest level. According to the statistics on high-frequency vibration, about 30% of vibration responses exceed 68 dB when using DTVI2 fasteners and Cologne-egg fasteners, which are concentrated within the range of 20 m from the tunnel center line. In the case that Lord fasteners are adopted, this index is reduced to 25%, while the vibration levels at any position are lower than 68 dB using Vanguard fasteners.

According to the above analysis, it can be concluded that Vanguard fasteners are able to significantly reduce the high-frequency environmental vibration caused by rail corrugation. Therefore, in the rail corrugation treatment, Vanguard fasteners can be considered to replace the fastener system besides rail grinding, so that the high-frequency vibration can be effectively suppressed when rail corrugation occurs again.

To explore the relationship between high-frequency environmental vibration and fastener parameters, the stiffness and damping are set to 5–100 kN/mm and 1–1000 kN·s/m, respectively. The ground vibration at the maximum point is taken as the analysis object, and high-frequency vibration changes at 250 Hz are compared with low-frequency ones at 31.5 Hz, 40 Hz, and 50 Hz. The results shown in Figs. 11 and 12 suggest that, in the entire analysis range, the variation of high-frequency vibration with stiffness and damping is similar to that of low-frequency vibration. However, there are obvious differences within the commonly used range.

Different from the phenomenon that the low-frequency vibrations first increase and then decrease with rising fastener stiffness, the high-frequency vibration at 250 Hz keeps

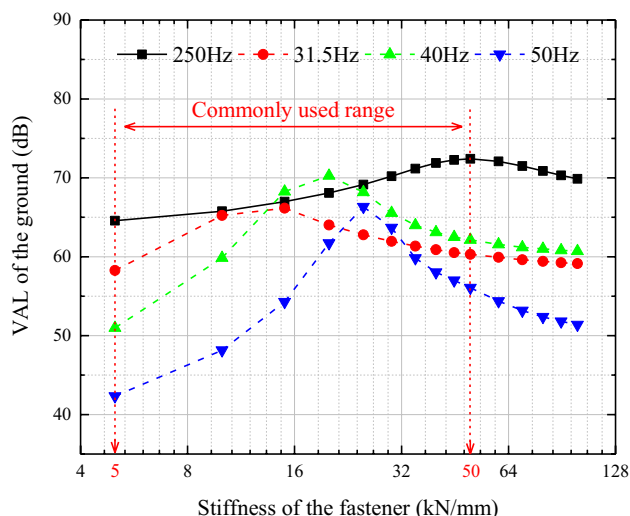


Fig. 11 Ground vibration under different stiffness

increasing in the commonly used range. However, there is a strong nonlinear correlation between the high-frequency vibration and fastener damping. The vibration response first decreases and then increases with the increase of damping, and the inflection point is about 10–20 kN·s/m, which is obviously different from the negative correlation between low-frequency vibrations and damping. The above results can be used to explain why the high-frequency vibration on the ground under the Vanguard fasteners is the lowest. Besides, an important conclusion can be drawn that the treatment of high-frequency environmental vibration caused by rail corrugation and low-frequency vibration has to be carried out following different principles. The fastener system

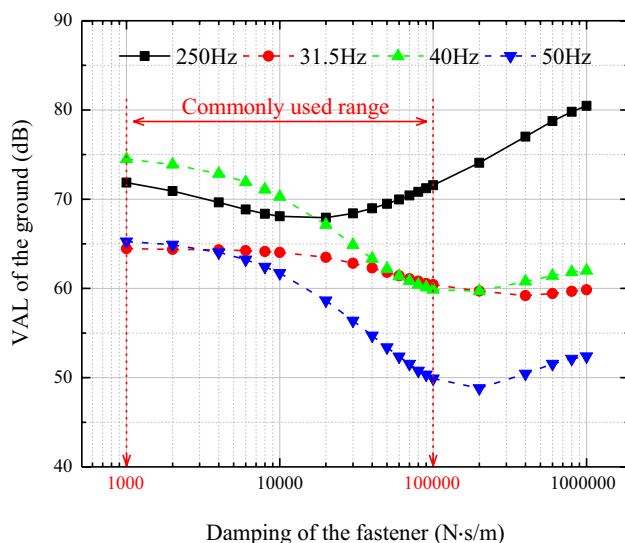


Fig. 12 Ground vibration under different damping

with temperate damping and lower stiffness should be selected for the elimination of high-frequency vibrations.

Conclusion

In this paper, a hybrid numerical analysis model consisting of a 3D load generation subsystem and a 2D wave propagation subsystem was proposed and validated by measured data. The effects of high-frequency vibration at 250 Hz induced by rail corrugation with different tunnel depths and rail fasteners were further analyzed. The results can provide an important theoretical reference for subway design and the remediation of rail corrugation. The main conclusions are drawn as follows:

- (1) Through the comparison with the measured data, it is proved that the hybrid numerical analysis model proposed in this study is able to accurately predict the attenuation trend of subway-induced environmental vibrations, especially in the high-frequency range caused by rail corrugation.
- (2) Under different tunnel depths, the high-frequency vibrations at 250 Hz induced by rail corrugation are transmitted to the ground by the dominant transmission path with the same angle of about 75° and 35°. In the case that the buried depth increases from 17 to 29 m, the 250 Hz vibration above the tunnel can be reduced by 5 dB. However, more serious high-frequency effects will appear in the vibration amplification region, especially at around 30 m away from the track where the 250 Hz vibration increases by 5.6 dB.
- (3) The variation of high-frequency vibration with fastener stiffness and damping in the commonly used range is quite different from that of low-frequency vibration. Specially, there is a significant nonlinear relationship between fastener damping and high-frequency vibration, and the optimal damping is about 10–20 kN·s/m.

Author contribution Sen Wang: formal analysis, data curation, writing—original draft, writing—review and editing, investigation. Tao Xin: conceptualization, methodology, formal analysis, writing—review and editing, funding acquisition. Pengsong Wang: data curation, writing—original draft, writing—review and editing. Yi Yang: writing—review and editing, investigation. Peng Chen: project administration, data curation. Lei Zhao: project administration, investigation, funding acquisition. Sihe Zhao: investigation, data curation. Yuming Luo: supervision, investigation.

Funding This work was supported by the Beijing Nova Program (Z191100001119126), the Fundamental Research Funds for the Central Universities (2020JBM049), the Shanghai Key Laboratory of Rail

Infrastructure Durability and System Safety (R202101) and the 111 Project (B20040).

Data availability The datasets used and analyzed during the current study are available from the corresponding author on reasonable request.

Declarations

Ethics approval and consent to participate Not applicable.

Consent for publication Not applicable.

Competing interests The authors declare no competing interests.

References

- Chen GX, Liu XZ (2004) Testing study on ratio of dynamic shear moduli and ratio of damping for recently deposited soils in Nanjing and its neighboring areas. *Chinese J Rock Mech Eng* 23:1403–1410
- Chen GX, Zhou ZR, Ouyang H, et al (2010) A finite element study on rail corrugation based on saturated creep force-induced self-excited vibration of a wheelset-track system. *J Sound Vib* 329. <https://doi.org/10.1016/j.jsv.2010.05.011>
- Collette C, Vanhoneracker P, Bastaitis R, Levy D (2008) Comparison between time and frequency studies of a corrugated curve of RER Paris network. *Wear* 265:1249–1258. <https://doi.org/10.1016/j.wear.2008.01.030>
- Connolly DP, Marecki GP, Kouroussis G et al (2016) The growth of railway ground vibration problems — a review. *Sci Total Environ* 568:1276–1282. <https://doi.org/10.1016/j.scitotenv.2015.09.101>
- Eadie DT, Santoro M, Oldknow K, Oka Y (2008) Field studies of the effect of friction modifiers on short pitch corrugation generation in curves. *Wear* 265:1212–1221. <https://doi.org/10.1016/j.wear.2008.02.028>
- Feng CC, Liu XL, Li W et al (2018) Influence of short pitch rail corrugation on interior noise of metro vehicles. *Noise Vib Control* 38:113–117
- Grassie SL (2009) Rail corrugation: characteristics, causes, and treatments. *Proc Inst Mech Eng Part F J Rail Rapid Transit* 223. <https://doi.org/10.1243/09544097JRR264>
- Grassie SL, Kalousek J (1993) Rail corrugation: characteristics, causes and treatments. *Proc Inst Mech Eng Part F J Rail Rapid Transit* 207. https://doi.org/10.1243/PIME_PROC_1993_207_227_02
- Hall JF (2018) Performance of viscous damping in inelastic seismic analysis of moment-frame buildings. *Earthq Eng Struct Dyn* 47:2756–2776
- Han M, Jiang J, Du H, Feng S (2021) Research on Damping Engagement Methodology in Dynamic Analysis of Isolated Structure. *Shock Vib* 2021:1–17. <https://doi.org/10.1155/2021/6613952>
- Huang Q, Huang H, Ye B et al (2017) Dynamic response and long-term settlement of a metro tunnel in saturated clay due to moving train load. *Soils Found* 57:1059–1075. <https://doi.org/10.1016/j.sandf.2017.08.031>
- ISO 3095–2005 (2005) Acoustics–Railway applications–Measurement of noise emitted by railbound vehicles
- Jin QY, Thompson DJ, Lurcock DEJ et al (2018) A 2.5D finite element and boundary element model for the ground vibration from trains in tunnels and validation using measurement data. *J Sound Vib* 422:373–389. <https://doi.org/10.1016/j.jsv.2018.02.019>

- Jin XS, Wen ZF, Zhang WH, Shen ZY (2005) Numerical simulation of rail corrugation on a curved track. *Comput Struct* 83 <https://doi.org/10.1016/j.compstruc.2005.03.012>
- Kouroussis G, Pauwels N, Brux P et al (2014) A numerical analysis of the influence of tram characteristics and rail profile on railway traffic ground-borne noise and vibration in the Brussels Region. *Sci Total Environ* 482–483:452–460. <https://doi.org/10.1016/j.scitotenv.2013.05.083>
- Kouroussis G, Vogiatzis KE, Connolly DP (2017) A combined numerical/experimental prediction method for urban railway vibration. *Soil Dyn Earthq Eng* 97:377–386. <https://doi.org/10.1016/j.soildyn.2017.03.030>
- Kuo KA, Verbraken H, Degrande G, Lombaert G (2016) Hybrid predictions of railway induced ground vibration using a combination of experimental measurements and numerical modelling. *J Sound Vib* 373:263–284. <https://doi.org/10.1016/j.jsv.2016.03.007>
- Kurzeck B, Hecht M (2010) Dynamic simulation of friction-induced vibrations in a light railway bogie while curving compared with measurement results. *Veh Syst Dyn* 48:121–138. <https://doi.org/10.1080/00423111003669045>
- Liu JB, Yin G, Du YX (2006) Consistent viscous-spring artificial boundaries and viscous-spring boundary elements. *Chinese J Geotech Eng* 28:1070–1075
- Liu WN, Ren J, Liu WF et al (2011) Analysis of rail corrugation tests in Beijing subway. *Urban Rapid Rail Transit* 24:6–9
- Liu XZ, Chen GX, Hu QX (2002) Primary study on dynamic shear modulus and damping ratio of recently deposited soil in area of Nanjing. *Earthq Eng Eng Vib* 22:127–131
- Lopes P, Costa PA, Ferraz M et al (2014) Numerical modeling of vibrations induced by railway traffic in tunnels: from the source to the nearby buildings. *Soil Dyn Earthq Eng* 61–62:269–285. <https://doi.org/10.1016/j.soildyn.2014.02.013>
- Lopes P, Ruiz JF, Alves Costa P et al (2016) Vibrations inside buildings due to subway railway traffic. Experimental validation of a comprehensive prediction model. *Sci Total Environ* 568:1333–1343. <https://doi.org/10.1016/j.scitotenv.2015.11.016>
- Ma M, Liu WN, Sun N, Bin WW (2014) Reasons and laws of ground vibration amplification induced by vertical dynamic load. *J Cent South Univ* 21:1660–1671
- Mazilu T (2010) Prediction of the interaction between a simple moving vehicle and an infinite periodically supported rail - Green's functions approach. *Veh Syst Dyn* 48:1021–1042. <https://doi.org/10.1080/00423110903248694>
- Meehan PA, Batten RD, Bellette PA (2016) The effect of non-uniform train speed distribution on rail corrugation growth in curves/corners. *Wear* 366–367:27–37. <https://doi.org/10.1016/j.wear.2016.05.009>
- Ng AK, Martua L, Sun G (2019) Influence of sleeper distance on rail corrugation growth. *Int Conf Intell Rail Transp ICIRT* 2018:1–5. <https://doi.org/10.1109/ICIRT.2018.8641668>
- Oostermeijer KH (2008) Review on short pitch rail corrugation studies. *Wear* 265:1231–1237. <https://doi.org/10.1016/j.wear.2008.01.037>
- Qi LF, Wang AB, Xie YS et al (2019) Influence of different track structures in metro systems on the tunnel and ground vibration characteristics QI. *Noise Vib Control* 39:147–152
- Sadeghi J, Esmaeili MH, Akbari M (2019) Reliability of FTA general vibration assessment model in prediction of subway induced ground borne vibrations. *Soil Dyn Earthq Eng* 117:300–311. <https://doi.org/10.1016/j.soildyn.2018.11.002>
- Sanayei M, Maurya P, Moore JA (2013) Measurement of building foundation and ground-borne vibrations due to surface trains and subways. *Eng Struct* 53:102–111. <https://doi.org/10.1016/j.engstruct.2013.03.038>
- Shen YK (2007) Study on the propagation laws of subway-induced vibration and isolation or reduction method of building vibration. Dissertation, Tongji University
- Shih JY, Thompson DJ, Zervos A (2017) The influence of soil non-linear properties on the track/ground vibration induced by trains running on soft ground. *Transp Geotech* 11:1–16. <https://doi.org/10.1016/j.trgeo.2017.03.001>
- Shih JY, Thompson DJ, Zervos A (2016) The effect of boundary conditions, model size and damping models in the finite element modelling of a moving load on a track/ground system. *Soil Dyn Earthq Eng* 89:12–27. <https://doi.org/10.1016/j.soildyn.2016.07.004>
- Sroczyński J, UrbańskaBonenberg L, Kumaszcza F, Turczyński B (1978) Spectrum character of vibration and clinical form of vibration disease. *Med Pr* 29:193–200
- Sutinen P, Zou J, Hunter LL, et al (2007) Vibration-Induced Hearing Loss. *Otol Neurotol* 28:171–177. <https://doi.org/10.1097/MAO.0b013e31802e29f2>
- Wu TX, Thompson DJ (2005) An investigation into rail corrugation due to micro-slip under multiple wheel/rail interactions. *Wear* 258:1115–1125. <https://doi.org/10.1016/j.wear.2004.03.060>
- Xin T, Wang S, Gao L et al (2020) Field measurement of rail corrugation influence on environmental noise and vibration: a case study in China. *Meas J Int Meas Confed* 164:108084. <https://doi.org/10.1016/j.measurement.2020.108084>
- Xing MT, Zhao C.Y., Wang P, et al (2019) A numerical analysis of ground vibration induced by typical rail corrugation of underground subway. *Shock Vib* 2019. <https://doi.org/10.1155/2019/8406813>
- Xu QY, Xiao ZC, Liu T et al (2015) Comparison of 2D and 3D prediction models for environmental vibration induced by underground railway with two types of tracks. *Comput Geotech* 68:169–183. <https://doi.org/10.1016/j.compgeo.2015.04.011>
- Yang J, Zhu S, Zhai W et al (2019) Prediction and mitigation of train-induced vibrations of large-scale building constructed on subway tunnel. *Sci Total Environ* 668:485–499. <https://doi.org/10.1016/j.scitotenv.2019.02.397>
- Yang YB, Liang XJ, Hung HH, Wu YT (2017) Comparative study of 2D and 2.5D responses of long underground tunnels to moving train loads. *Soil Dyn Earthq Eng* 97:86–100. <https://doi.org/10.1016/j.soildyn.2017.02.005>
- Zhang B (2002) Engineering practice and theoretical analysis on vibration control of shallow underground engineering and related systems. Dissertation, China Academy of Railway Sciences
- Zhao CY, Wang P, Yi Q (2017) Internal noise reduction in railway vehicles by means of rail grinding and rail dampers. *Noise Control Eng J* 65:1–13. <https://doi.org/10.3397/1/376421>
- Zhu ZH, Liu YB, Wang LD et al (2020) Analysis of ground random vibration induced by subway transit based on 2.5-dimensional finite element and pseudo excitation methods. *China Railw Sci* 41:29–39

Publisher's note Springer Nature remains neutral with regard to jurisdictional claims in published maps and institutional affiliations.